Journal of Dynamics, Monitoring and Diagnostics, 2024, 3, 49-58
https://doi.org/10.37965/jdmd.2024.484

ISTP
RESEARCH ARTICLE

A Comprehensive 3-Steps Methodology for Vibration-Based Fault Detection, Diagnosis and Localization in Rotating Machines

Khalid M. Almutairi and Jyoti K. Sinha
Dynamics Laboratory, School of Engineering, The University of Manchester, Manchester M13 9PL, UK

(Received 06 December 2023; Revised 20 February 2024; Accepted 25 March 2024; Published online 25 March 2024)

Abstract: In any industry, it is the requirement to know whether the machine is healthy or not to operate machine further. If the machine is not healthy then what is the fault in the machine and then finally its location. The paper is proposing a 3-Steps methodology for the machine fault diagnosis to meet the industrial requirements to aid the maintenance activity. The Step-1 identifies whether machine is healthy or faulty, then Step-2 detect the type of defect and finally its location in Step-3. This method is extended further from the earlier study on the 2-Steps method for the rotor defects only to the 3-Steps methodology to both rotor and bearing defects. The method uses the optimised vibration parameters and a simple Artificial Neural Network (ANN)-based Machine Learning (ML) model from the earlier studies. The model is initially developed, tested and validated on an experimental rotating rig operating at a speed above 1st critical speed. The proposed method and model are then further validated at 2 different operating speeds, one below 1st critical speed and other above 2nd critical speed. The machine dynamics are expected to be significantly different at these speeds. This highlights the robustness of the proposed 3-Steps method.

Keywords: bearing faults; fault diagnosis; machine learning; rotating machines; rotor faults; vibration analysis

I. INTRODUCTION

Industries and power plants crucially depend on the seamless operation of rotating machinery, making the early and accurate detection of associated faults vital [1]. These machines encompass various integrated components, including rotors, bearings, supporting structures, and electric motors, all of which are susceptible to numerous malfunctions due to manufacturing and installation imperfections and inevitable wear and tear from daily operation [2,3].

Common faults, including rotor misalignment, mass imbalance, cracks, shaft bends, and inadequate bearing lubrication, significantly impact the reliability and performance of these essential machines [4–6]. These rotor and bearing faults often result in high vibrations, damaging critical components and, in severe cases, complete machine failure [7]. Therefore, developing effective methodologies for early fault detection and diagnosis is imperative to enhance machine reliability, prevent failures, and ensure cost-effective maintenance.

Over the years, vibration-based condition monitoring (VCM) has proven to be a reliable technique for detecting and diagnosing faults in rotors and bearings [8,9]. The analysis of vibration signals, which are sensitive to changes in structural parameters and varied fault conditions, provides valuable insights into the health status of rotating machinery. Vibration signal features have been extensively studied for classifying different fault types in rotating machinery. Additionally, these vibration features have been integrated with machine learning algorithms, like artificial neural networks (ANN) and support vector machines (SVM), to enable more efficient classification and differentiation of machinery fault levels or types [10–13]. With the advent of Artificial Intelligence (AI) and Machine Learning (ML), there has been significant progress in developing intelligent diagnostic systems and accelerating decision-making processes with minimal human intervention [14–17].

Li *et al.* [18] proposed a novel statistical feature extraction and evaluation method for rotating machinery fault diagnosis. They extracted statistical features by computing the sample average of raw features from multiple arbitrarily selected partitions of the vibration signal. According to the central limit theorem, these statistical features will follow normal distributions. Experiments showed that statistical features significantly improved the classification accuracy compared to raw features for ANN and support vector machine (SVM) classifiers on a machinery fault simulator. The proposed method provided an accurate diagnosis of common faults like unbalance and bearing faults only.

Espinoza-Sepulveda and Sinha [19] presented a method for identifying rotor defects based on the analysis of rotor vibration measurements collected in an experimental lab. Their methodology is based on artificial intelligence (AI) and utilizes a machine learning (ML) model. Their primary research objective was to optimize parameters derived from vibration data to detect rotor defects. They used an artificial neural network (ANN) model to classify these defects, demonstrating the applicability of AI and vibration features in machinery fault detection.

Natalia Espinoza-Sepulveda *et al.* [20] proposed a rotor faults identification method that relies on rotor vibration measurements from an experimental lab rig and implemented an artificial intelligence (AI)-based machine learning

Corresponding authors: Khalid M. Almutairi (e-mail: khalid.almutairi@manchester.ac.uk); and Jyoti K. Sinha (e-mail: jyoti.sinha@manchester.ac.uk).

(ML) model. The identification method has two main steps: the first identifies if the rotor is healthy or faulty, and the second specifies the exact nature of the rotor fault. The method successfully identified the healthy condition and four rotor faults: looseness, rotor-stator rub, misalignment, and shaft bow.

Khalid and Sinha [21] have expanded the vibration-based machine learning (VML) model of the previous study [19] to detect faults in both rotors and anti-friction bearings. The vibration parameters have been revised by extending the frequency range to cover bearing resonance responses from bearing defects. The proposed VML method was first developed on an experimental rig at one speed above the first critical speed and accurately diagnosed all machine conditions. To further evaluate the method's usefulness and robustness, it was tested at a speed below the first critical speed and another rotating speed above the second critical speed, where machine dynamics differ significantly. The vibration parameters and ANN model accurately identified the healthy condition, misalignment, shaft crack, shaft rub and bearing fault.

This research builds upon and extends the previous research study of the 2-Steps method [20] into a comprehensive 3-Steps methodology to identify the machine condition (healthy or not), diagnose and locate the rotating machine's faults. The proposed 3-Steps methodology for the machine fault diagnosis is intended to meet the industrial requirements to aid the maintenance activity. The Step-1 identifies whether machine is healthy or faulty, then Step-2 detect the type of defect and finally its location in Step-3. It is in line with industrial the requirement to know whether the machine is healthy or not to operate machine further. If the machine is not healthy then what is the fault in the machine and then finally its location. The proposed method is using the vibration parameters estimated from the measured vibration responses and then smart detection process in all 3-Steps through a machine learning model (ML) [21].

First, a dataset of vibration features is used to classify healthy and faulty states. Then, if the machine is faulty, the classifier identifies the exact type of fault. Finally, the third step is to pinpoint the location of some of the identified faults. The refined method not only addresses rotor-related faults, but also incorporates anti-friction bearing faults. This paper utilizes vibration data from a laboratory-scale rig at various operating speeds. The proposed 3-Steps method is developed at a rotor speed which is above the 1st critical speed. The model is further tested and validated at other two different rotating speeds, one below 1st critical speed and other above 2nd critical speed. The dynamics of the machine are different at these speeds, but the proposed model provides encouraging results. This research enhances the existing AI and ML models for fault identification, providing a valuable contribution to the field of predictive maintenance and fault diagnosis in industrial rotating machines.

This paper is structured as follows: Section II presents the methodology of the proposed 3-Steps method. Section III describes the experimental setup and data collection process. Section IV presents the extracted vibration features, and Sections V and VII delve into the data analysis and results, respectively, highlighting the study's key findings. Finally, Section VII concludes the paper, summarizing the main points.

II. METHODOLOGY

A 3-Steps fault identification and diagnosis approach for rotors and bearings is proposed using a multi-layer perceptron (MLP) artificial neural network (ANN) of a previous study [20].

The 1st step determines if the asset is healthy or faulty based on the input data propagated through the MLP network architecture. The output layer contains two possible classifications – healthy or faulty. If a fault is detected,

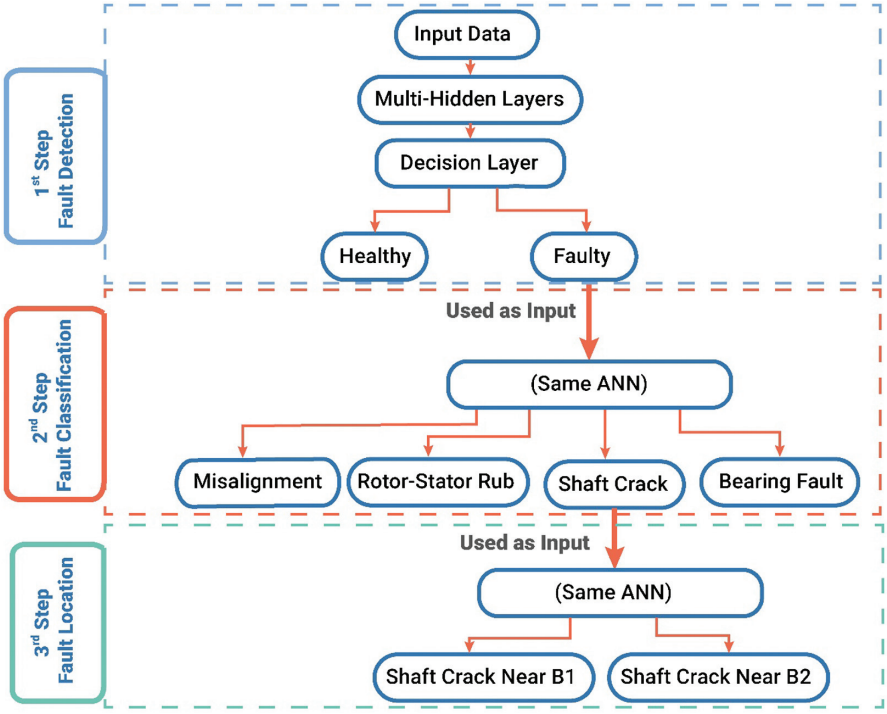

Fig. 1. A schematic diagram of the 3-Steps method using ANN.

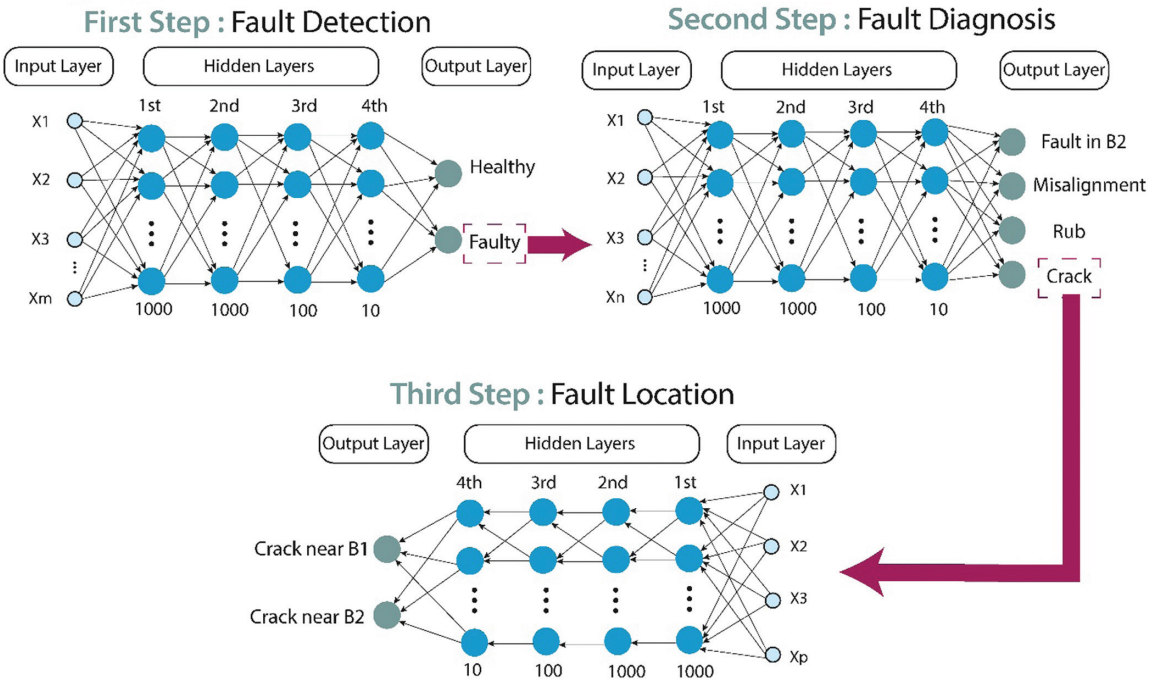

Fig. 2. Schematic representation of the supervised four-hidden-layer ANN classification process.

the 2nd step identifies the precise nature of the fault using the same MLP network. The fault types are misalignment, shaft crack, rotor-stator rub, and bearing faults. This knowledge enables targeted maintenance activities to mitigate failure risk. Only faulty data are used in the 2nd step. The 3rd step localizes the fault by pinpointing its location on the rotor or bearing assembly. Potential discrete fault locations such as shaft crack in location 1 and shaft crack in location 2 are classified. The ANN architectures used in all steps are identical. The idea is to make this simple ANN model as a standard model for all faults detection but by using the vibration and rotordynamics-based parameters. Figure 1 shows a schematic diagram of the 3-Steps method using ANN, and Fig. 2 represents the supervised four-hidden-layer ANN classification process.

Table I and Fig. 2 outline that the MLP network is architecturally structured with four hidden layers. Each layer comprises multiple neurons, with the hidden layers containing 1000, 1000, 100, and 10 neurons, respectively. The hyperbolic tangent sigmoid function [10] is the chosen activation function for these hidden layers, while the output layer implements a Softmax function [11], providing a normalized exponential function. The ANN was trained using a supervised learning approach, where the model was provided with input data (vibration features) and the correct output. A Scaled Conjugate Gradient Back-Propagation training function is employed with Cross-Entropy as the performance function, ensuring optimal network performance through iterative training phases. It is important to note that the input data in the 1st Step contain all data, only fault state data in 2nd Step, and the data related to a particular fault in the 3rd Step are used to reduce the computational effort and to also support the optional and maintenance within any industry.

Table I. Characteristics and configuration of the implemented neural network model

Parameter	Specification
Architecture	Four-hidden-layer feed-forward neural network
Activation function (Hidden neurons)	Hyperbolic tangent sigmoid
Transfer function (Output neurons)	Normalised exponential function (Softmax)
Training function	Scaled conjugate gradient back-propagation
Performance function	Cross-entropy

III. EXPERIMENTAL RIG

An experimental rig was constructed to generate vibration data for different operating conditions and speeds (Figs. 3 and 4). The rig consists of two steel shafts, denoted as Sh1 and Sh2, coupled by a rigid flanged sleeve coupling. Sh1 is 1000 mm long, and Sh2 is 500 mm long, both with a diameter of 20 mm. Each shaft is supported by two deep groove ball bearings mounted in cast iron housings (Table IV). The bearings are secured inside pedestals attached to the steel baseplate using four springs per bearing. Sh1 has two steel balancing discs, each with a diameter of 125 mm and a thickness of 14 mm. Sh2 has one identical balancing disc. Discs are secured on the shafts using locking nuts and can be adjusted to introduce controlled imbalance.

Vibration data is acquired by Luwei [22] using four accelerometers (Model: 352C33, 100 mV/g sensitivity) attached to the bearing housings using stud mounts. Accelerometers are oriented at 45° to the horizontal axis. The accelerometers are connected to a data acquisition system with anti-aliasing filters.

A 0.75 kW induction motor coupled to the rig via flexible couplings is used to rotate the shaft up to 3000

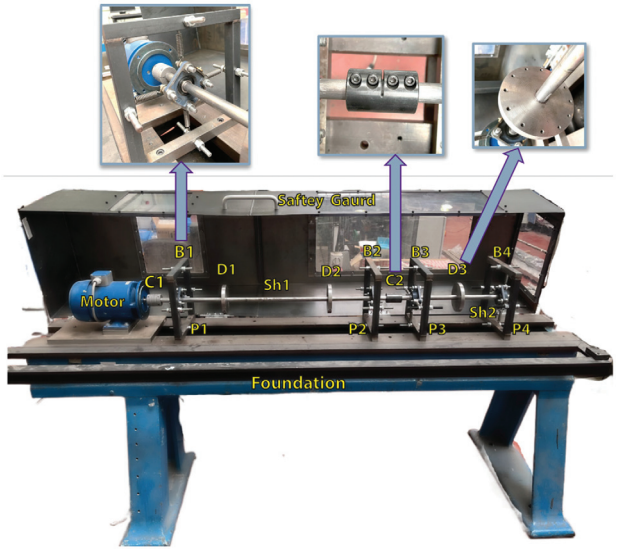

Fig. 3. Experimental rig setup.

RPM. Elastic couplings help isolate experimental vibration from motor noise.

The rig was run at 450 RPM (7.5 Hz), 900 RPM (15 Hz) and 1350 RPM (22.5 Hz). These speeds were selected based on the first two bending critical speeds at 11.52 Hz and 18.62 Hz identified by the modal tests [22]. The experimental modeshapes (from coupling location, C1 to the end of the shaft) [22] at these 2 natural frequencies are shown in Fig. 5. The chosen speeds are below, between, and above the critical speeds. The dynamics of the rotating rig differ significantly at these 3 speeds as clear from the modeshapes. Five conditions were tested at each speed: healthy, misalignment, shaft crack near B1, shaft crack near B2, shaft rub near D1, and defective bearing (B2). For each condition, 40 runs were performed with a 10 kHz sampling rate. Tables II and III show the number of samples and, descriptions of each condition and the description of the simulated faults in the experimental rig. The ball bearing specifications utilized in the test rig are shown in Table IV.

Table V summarizes the calculated frequencies corresponding to the ball, inner race, outer race, and cage components of the bearings at various speeds, supporting

Table II. Samples of various machine conditions at each tested speed

Machine condition	Number of runs (Samples)		
	450 RPM	900 RPM	1350 RPM
Healthy (residual unbalance and residual misalignment)	40	40	40
Misalignment	40	40	40
Crack near B1	40	40	40
Crack near B2	40	40	40
Rotor rub	40	40	40
Faulty bearing	40	40	40

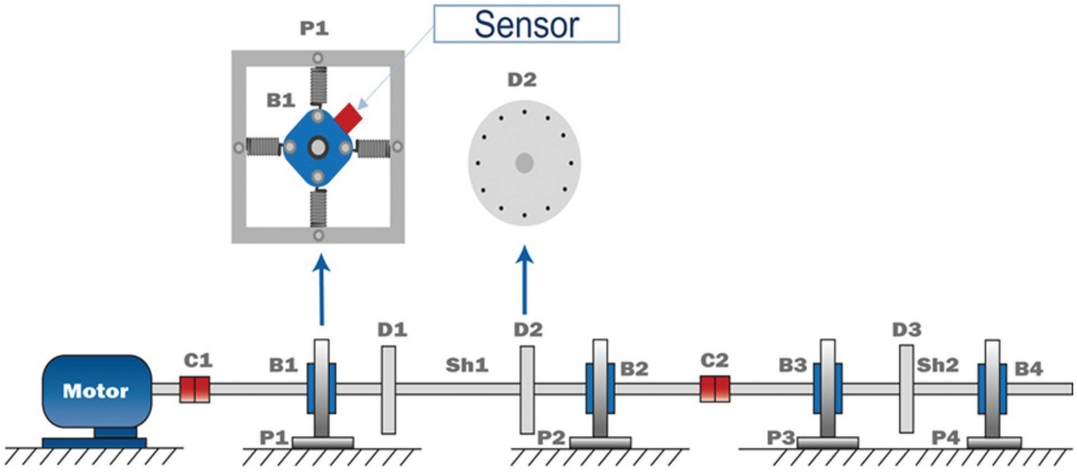

Fig. 4. Schematic diagram of the experimental rig.

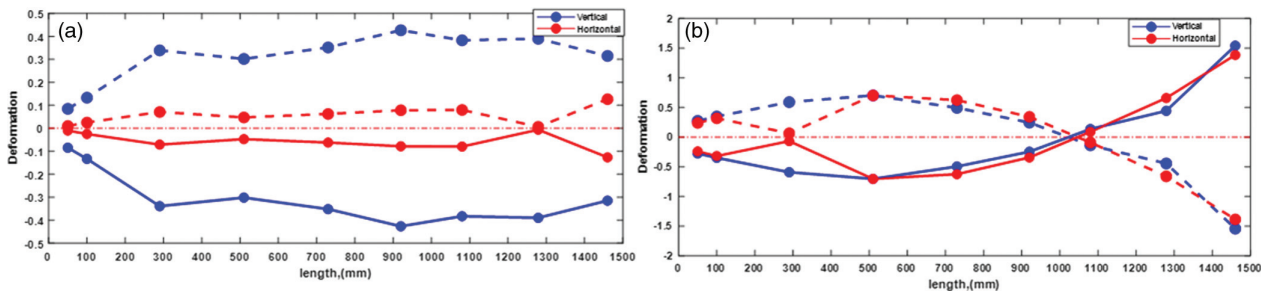

Fig. 5. Experimental modeshapes at the natural frequencies, 11.52 Hz and 18.62 Hz.

Table III. Descriptions of various machine conditions at each tested speed

Machine condition	Description
Healthy (residual unbalance and residual misalignment)	Residual misalignment and residual unbalance.
Misalignment	Parallel Misalignment with vertical displacement of B1 of 0.8 mm.
Crack near B1	On the rotor near B1, a 0.33 mm shim is pasted into a 0.34 mm wide by 4 mm deep notch.
Crack near B2	On the rotor near B2, a 0.33 mm shim is pasted into a 0.34 mm wide by 4 mm deep notch.
Rotor rub	Perspex blade on rotor near D1.
Faulty bearing	Bearing cage defect at B2.

Table IV. Ball bearing specification

Bearing parts	Specification
Inner (bore) diameter (d_i)	20 mm
Pitch circle diameter (d_p)	33.50 mm
Diameter of roller (d_b)	7.938 mm
The contact angle of the roller (β)	0
Number of rollers (n_r)	10

the experimental rotor system. The calculated frequencies based on the equations are provided in [9].

IV. VIBRATION DATA PROCESSING AND FEATURES EXTRACTION

A previous study [21] optimised the selection of the vibration features to be used in the machine learning model for reliable and accurate rotor and bearing diagnosis. The optimized features combine time and frequency domain features extracted from the measured vibration responses. In the time domain, the root mean square (RMS) of acceleration represents the signal's overall energy, while kurtosis (K) of acceleration provides information regarding the shape distribution of the sample. The frequency range for RMS calculation is extended to 5000 Hz to include bearing resonance related vibration responses. Kurtosis focuses on 2000–5000 Hz to reflect the bearing condition. In the frequency domain, the velocity vibration amplitudes at 1×, 2× and 3× of shaft rotating frequency for the rotor faults. Spectrum energy (SE) of velocity measures vibration content related to the rotor and bearing faults from 0.3× rotational speed to 5000 Hz. These 6 features per bearing at the 3 rotating speeds were extracted from each data sample. Table VI summarises the extracted features from vibration data to be used as the input of the proposed method.

Table V. Characteristic frequencies of ball bearing used in the experimental rig

Rotor speed (RPM)			
Condition	**450**	**900**	**1350**
The relative speed between the inner race and the outer race (Hz)	7.5	15	22.5
Frequency related to the ball defect (Hz)	29.87	59.75	89.62
Frequency related to a defect in the inner race (Hz)	37.11	74.22	111.33
Frequency related to a defect in the outer race (Hz)	22.89	45.78	68.67
Frequency related to a defect in the cage (Hz)	2.86	5.72	8.58

V. VIBRATION DATA ANALYSIS AT ROTATING SPEED, 15 HZ

The measured vibration acceleration data are analysed in both time and frequency domains. Figures 6–8 show a

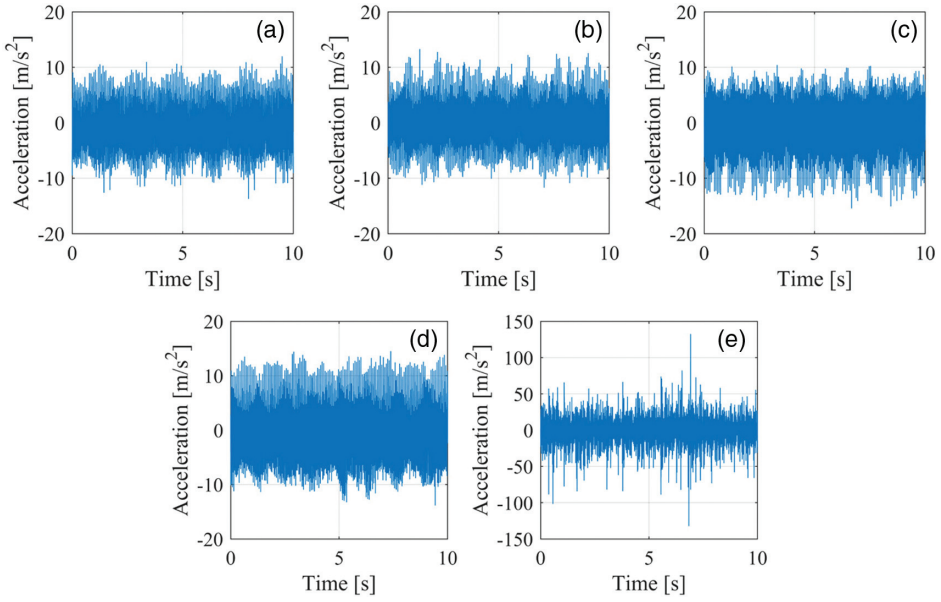

Fig. 6. Typical time domain waveform at B2 for the different machine faulty conditions at a rotating speed of 15 Hz: (a) Misalignment, (b) Crack near B1, (c) Crack near B2, (d) Rub, and (e) Fault in B2.

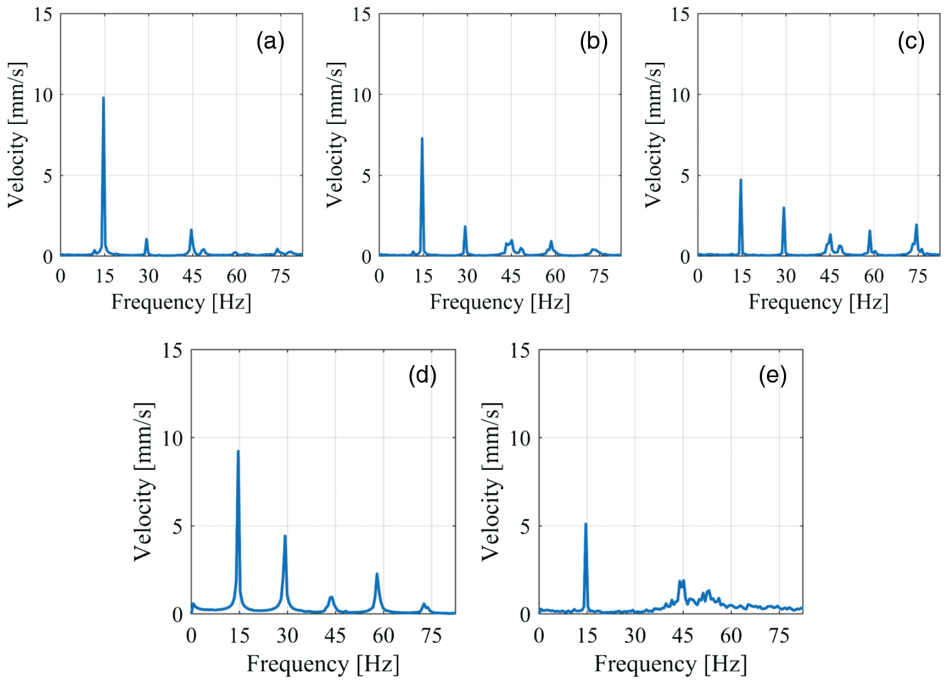

Fig. 7. Typical velocity vibration spectra at B2 for the different machine faulty conditions at rotating speed 15 Hz: (a) Misalignment, (b) Crack near B1, (c) Crack near B2, (d) Rub, and (e) Fault in B2.

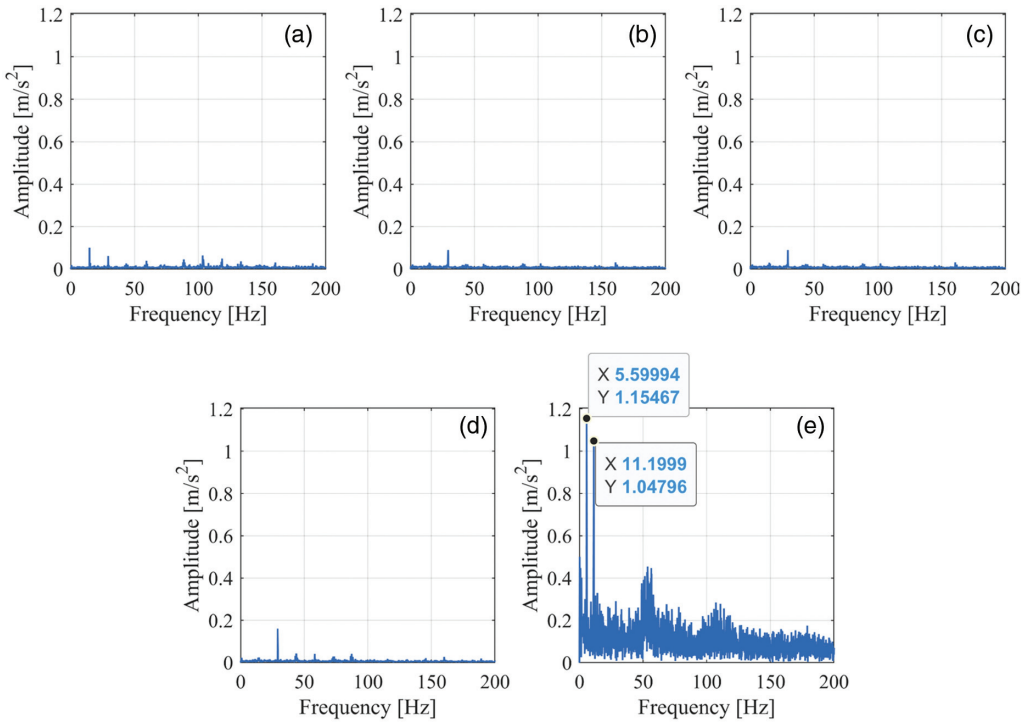

Fig. 8. Typical envelope spectra at B2 for faulty machine conditions at a rotating speed of 15 Hz: (a) Misalignment, (b) Crack near B1, (c) Crack near B2, (d) Rub, and (e) Fault in B2.

typical comparative vibration analysis of a machine with experimentally simulated rotor and bearing defects at 15 Hz at the bearing, B2.

In the time domain (Fig. 6), the acceleration vibration signals show changes in amplitude over time but doesn't reveal much about the fault type. The velocity spectra (Fig. 6) show peaks at 1×, 2×, and 3× (the first, second, and third harmonics of the rotational speed) with different amplitudes for the rotor fault conditions in Fig. 7(a–d). However, there is no obvious bearing fault related

frequencies are observed in Fig. 6e for the defective bearing B2.

To further confirm the presence of the defect in the bearing B2, the envelope analyses are carried out for all vibration data. The vibration acceleration signals are initially passed through a bandpass filtered from 2000 to 5000 Hz to get the vibration data around the bearing assembly resonance frequency region. The envelope analysis via Hilbert Transform [23] is then carried out on the filtered signals. The spectra of the envelope signals at the bearing, B2 are shown in Fig. 8. Figure 8e shows the presence of the cage related defect frequency of 5.6 Hz and its harmonics. Hence, this confirms the presence of defect in the bearing, B2. However, there is no such bearing defective frequency peaks are observed for other rotor related fault conditions as obvious from Fig. 8(a–d). This confirms that the rotor fault conditions are not having the bearing defects.

VI. THE APPLICATION OF THE 3-STEPS METHODOLOGY

A. INPUT DATA OF THE ML

The initial step focuses on classifying the machine's condition as either healthy or faulty. The input matrix, denoted as A, captures vibrational features across different bearings and conditions. Each row represents an individual sample run, while each column represents a feature (RMS, K, 1X, 2X, 3X, and SE) for each of the four bearings (B1, B2, B3, B4). The target matrix for this step is binary, reflecting each sample's healthy or faulty status. A '1' denotes a faulty condition, while a '0' signifies a healthy machine condition.

$$\boldsymbol{DataH} = [H_1 \;\; H_2 \;\; \ldots \;\; H_z]^T,$$
$$\boldsymbol{DataM} = [M_1 \;\; M_2 \;\; \ldots \;\; M_z]^T,$$
$$\boldsymbol{DataC_l} = [C_{l1} \;\; C_{l2} \;\; \ldots \;\; C_{lz}]^T,$$
$$\boldsymbol{DataC_r} = [C_{r1} \;\; C_{r2} \;\; \ldots \;\; C_{rz}]^T,$$
$$\boldsymbol{DataR} = [R_1 \;\; R_2 \;\; \ldots \;\; R_z]^T,$$
$$\boldsymbol{DataBF} = [BF_1 \;\; BF_2 \;\; \ldots \;\; BF_z]^T$$
$$\boldsymbol{A} = [\boldsymbol{DataH} \;\; \boldsymbol{DataM} \;\; \boldsymbol{DataC_l} \;\; \boldsymbol{DataC_r} \;\; \boldsymbol{DataR} \;\; \boldsymbol{DataBF}]^T \quad (1)$$

where ***DataH*** is the databank for the healthy condition, ***DataM*** is for misalignment fault, $\boldsymbol{DataC_l}$ is for cracked shaft near B1, $\boldsymbol{DataC_r}$ is for cracked shaft near B2, ***DataR*** is for rotor rub fault, and ***DataBF*** is for bearing fault. Each databank contains features from individual experimental runs, organized as follows:

$$\boldsymbol{H} = [RMS_{B1,z} \; K_{B1,z} \; 1x_{B1,z} \; 2x_{B1,z} \; 3x_{B1,z} \; SE_{B1,z} \; \ldots \; RMS_{B2,z} \; \ldots \; SE_{B2,z} \; RMS_{B3,z} \; \ldots \; SE_{B3,z} \; RMS_{B4,z} \; \ldots \; SE_{B4,z}] \quad (2)$$

where z is the run number for the healthy condition.

A subset matrix of the original matrix A is used for diagnosed faults. This matrix retains only those rows classified as faulty in Step-1. Each column in the subset matrix still represents specific features for each bearing, thus providing insights into the exact nature of the fault. The target matrix encompasses multiple classes, each representing a particular fault type, such as misalignment, shaft crack, rotor-stator rub, or bearing fault. Each faulty sample in the input matrix is associated with a category in this target matrix, facilitating a more detailed classification.

Upon detecting a shaft crack in Step-2, the matrix is derived to specify the fault's location further. The matrix retains data relevant to the crack condition and is structured similarly to matrix $\boldsymbol{A}$, although focusing on distinguishing between potential fault locations. The target for this step is to determine the potential location of the shaft crack, specifically whether it's closer to bearing B1 or B2. As such, the target matrix has binary outcomes signifying the location of the detected shaft crack.

The 3-Steps method provided in Section II is executed here. The samples (runs) described in Table II are organized into three datasets for the ML model's training, validation, and testing. 70% of the samples (runs) from machine conditions at 750 RPM, 900 RPM, and 1350 RPM are utilized for training the network, with the weights modified by the learning rule. 15% of the samples are then utilized for validation, which entails checking the trained network with these data until their classification error achieves a desired minimal error level. At this time, the training process is terminated. At this phase, the network's optimum weights have been determined, and the remaining 15% of anonymous data are evaluated to determine the network's generalization.

The data 70%-15%-15% (training-validation-testing) are applied to Step-1, Step-2 and Step-3 models. The model's performance is computed using Eq. (3).

Table VII. Overall performance of the 1st step, fault detection (%) of tested data of rotation machine at 15 Hz

		Target class	
		Healthy	**Faulty**
Output Class	Healthy	100	0
	Faulty	0	100

Table VI. Extracted vibration features

Features	Frequency range	Domain	Amplitude
Root mean square (RMS)	0 – 5000 Hz	Time	Acceleration
Kurtosis (*K*)	2000 – 5000 Hz	Time	Acceleration
The first harmonic of rotating speed (1×)	1×	Frequency	Velocity
The second harmonic of rotating speed (2×)	2×	Frequency	Velocity
The third harmonic of rotating speed (3×)	3×	Frequency	Velocity
Spectrum energy (*SE*)	0.3 Rotational speed – 5000 Hz	Frequency	Velocity

Table VIII. Overall performance of the 2nd step, fault diagnosis (%) of tested data of rotation machine at 15 Hz

		Target class			
		Misalignment	Shaft crack	Shaft rub	Bearing fault
Output Class	Misalignment	100	0	0	0
	Shaft Crack	0	100	0	0
	Shaft Rub	0	0	100	0
	Bearing Fault	0	0	0	100

$$Performance\ (\%) = \left(\frac{no.\ correct\ classification}{total\ of\ input}\right) \times 100\% \tag{3}$$

B. MODEL DEVELOPMENT

The proposed 3-Steps fault detection, diagnosis and location method was developed using vibration data acquired at 900 RPM (15 Hz). The data was divided into 70% training, 15% testing, and 15% validation sets. The method achieved 100% fault detection, diagnosis, and location accuracy for the training, testing, and validation data sets (Tables VII–IX). Specifically, the model perfectly classified the machine condition as healthy or faulty, diagnosed the fault type (misalignment, crack, rub, bearing fault), and located the fault (crack near B1 or B2).

C. MODEL VALIDATION

The developed method was validated by testing on the additional vibration data obtained at the rotating speed of 7.5 Hz and 22.5 Hz, which are below 1st and above 2nd critical speeds of the rotating machine, respectively. The data was separated into 70% training, 15% testing, and 15% validation sets for each validation speed. The method maintained 100% fault detection, diagnosis, and location accuracy at 7.5 Hz and 22.5 Hz for all data sets (Tables X–XV).

Despite varying dynamics at 2 different rotating speeds, the consistently high performance demonstrates the robustness of the extracted vibration features and the approach's effectiveness across operating conditions. The ability to precisely detect, diagnose, and localize faults highlights the novelty of the proposed 3-Steps process, providing an automated solution superior to thresholding. The results validate the viability of industrial applications, where early and accurate fault detection is critical.

Table IX. Overall performance of the 3rd step, fault location (%) of tested data of rotation machine at 15 Hz

		Target class	
		Shaft crack near B1	Shaft crack near B2
Output Class	Shaft Crack Near B1	100	0
	Shaft Crack Near B2	0	100

Table XII. Overall performance validation of the 3rd step at the machine rotation speed of 7.5 Hz

		Target class	
		Shaft crack near B1	Shaft crack near B2
Output Class	Shaft Crack Near B1	100	0
	Shaft Crack Near B2	0	100

Table X. Overall performance validation of the 1st step at the machine rotation speed of 7.5 Hz

		Target class	
		Healthy	Faulty
Output Class	Healthy	100	0
	Faulty	0	100

Table XIII. Overall performance of the 1st step showing further validation at rotating speed of 22.5 Hz

		Target class	
		Healthy	Faulty
Output Class	Healthy	100	0
	Faulty	0	100

Table XI. Overall performance validation of the 2nd step at the machine rotation speed of 7.5 Hz

		Target class			
		Misalignment	Shaft crack	Shaft rub	Bearing fault
Output Class	Misalignment	100	0	0	0
	Shaft Crack	0	100	0	0
	Shaft Rub	0	0	100	0
	Bearing Fault	0	0	0	100

Table XIV. Overall performance of the 2nd step showing further validation at rotating speed of 22.5 Hz

		Target class			
		Misalignment	**Shaft crack**	**Shaft rub**	**Bearing fault**
Output Class	Misalignment	100	0	0	0
	Shaft Crack	0	100	0	0
	Shaft Rub	0	0	100	0
	Bearing Fault	0	0	0	100

Table XV. Overall performance of the 3rd step showing further validation at rotating speed of 22.5 Hz

		Target class	
		Shaft crack near B1	**Shaft crack near B2**
Output Class	Shaft Crack Near B1	100	0
	Shaft Crack Near B2	0	100

VII. CONCLUDED REMARKS

This study presented a novel 3-Steps machine learning approach for automated rotor and bearing faults diagnosis of rotating machinery across different operating speeds with significantly different rotor dynamics. The proposed approach first identifies machine conditions as healthy or faulty using optimized vibration features as inputs to a multi-layer perceptron neural network in the 1st Step. This is important step for the management and operations teams to know whether they can run the machine or not. If a fault is detected, the 2nd Step identifies the precise fault type. This is demonstrated here for both rotor faults like misalignment, shaft cracks, shaft rub, and the bearing defects. This is an essential step for the vibration-based condition monitoring team to know the exact nature of the fault in the machine. Finally, the 3rd Step provides the location of the fault to support the maintenance team to carry out the remedial work efficiently. This has also been demonstrated through the example of the shaft cracks.

The method is initially developed and successfully demonstrated using experimental vibration data from a laboratory rotor-bearing test rig at a rotating speed above the 1st critical speed. The proposed 3-Steps method is then further validated at 2 different rotation speeds (one below 1st and other above 2nd critical speeds) having significantly different dynamics behaviours. This confirms the robustness of the proposed methodology and the vibration parameters used are truly represent the machine dynamics. The ANN model is kept simple and same for all steps. The idea is to standardise this model for all possible faults detection by the selecting the appropriate vibration parameters (features) based on the machine rotordynamics. The proposed 3-Steps method is simple and based on the rotordynsamics which has potential to use in the industries.

CONFLICT OF INTEREST STATEMENT

The authors declare no conflicts of interest.

REFERENCES

[1] Y. He, J. Guo, and X. Zheng, "From surveillance to digital twin: challenges and recent advances of signal processing for industrial internet of things," *IEEE Signal Process. Mag.*, vol. 35, no. 5, pp. 120–129, 2018.

[2] R. Tiwari, *Rotor Systems: Analysis and Identification*. Boca Raton, FL: CRC Press, 2017.

[3] P. Kumar and R. Tiwari, "A review: multiplicative faults and model-based condition monitoring strategies for fault diagnosis in rotary machines," *J. Braz. Soc. Mech. Sci. Eng.*, vol. 45, no. 5, p. 282, 2023.

[4] N. Rezazadeh et al., "Diagnosing and balancing approaches of bowed rotating systems: a review," *Appl. Sci.*, vol. 12, no. 18, p. 9157, 2022.

[5] L. Kuan et al., "Nonlinear dynamic behavior of a dual-rotor bearing system with coupling misalignment and rubbing faults," *Meas. Sci. Technol.*, vol. 34, no. 1, p. 014005, 2022.

[6] A.-T. W. K. Fahmi, K. R. Kashyzadeh, and S. Ghorbani, "A comprehensive review on mechanical failures cause vibration in the gas turbine of combined cycle power plants," *Eng. Failure Anal.*, vol. 134, p. 106094, 2022.

[7] A. Althubaiti, F. Elasha, and J. A. Teixeira, "Fault diagnosis and health management of bearings in rotating equipment based on vibration analysis–a review," *J. Vibroeng.*, vol. 24, no. 1, pp. 46–74, 2022.

[8] R. B. Randall, *Vibration-Based Condition Monitoring: Industrial, Automotive and Aerospace Applications*. Chichester, West Sussex: John Wiley & Sons, 2021.

[9] J. K. Sinha, *Industrial Approaches in Vibration-Based Condition Monitoring*. Boca Raton, FL: CRC Press, 2020.

[10] T. P. Vogl et al., "Accelerating the convergence of the back-propagation method," *Biol. Cybernet.*, vol. 59, pp. 257–263, 1988.

[11] C. M. Bishop and N. M. Nasrabadi,*Pattern Recognition and Machine Learning*, Vol. 4. New York, NY: Springer, 2006.

[12] S.-F. Yuan and F.-L. Chu, "Support vector machines-based fault diagnosis for turbo-pump rotor," *Mech. Syst. Signal Process.*, vol. 20, no. 4, pp. 939–952, 2006.

[13] S. Singh and N. Kumar, "Rotor faults diagnosis using artificial neural networks and support vector machines," *Int. J. Acoust. Vib.*, vol. 20, no. 3, pp. 153–159, 2015.

[14] V. Singh et al., "Artificial intelligence application in fault diagnostics of rotating industrial machines: a state-of-the-art review," *J. Intell. Manuf.*, vol. 34, no. 3, pp. 931–960, 2023.

[15] M. Akbari, H. Homaei, and M. Heidari, "An intelligent fault diagnosis approach for gears and bearings based on wavelet transform as a preprocessor and artificial neural networks," *Int. J. Math. Modell. Comput.*, vol. 4, no. 4 (FALL), pp. 309–329, 2014.

[16] T. Mian, A. Choudhary, and S. Fatima, "Multi-sensor fault diagnosis for misalignment and unbalance detection using

machine learning," *IEEE Trans. Ind. Appl.*, vol. 60, pp. 1–14, 2023.

[17] L. C. Brito et al., "An explainable artificial intelligence approach for unsupervised fault detection and diagnosis in rotating machinery," *Mech. Syst. Signal Process.*, vol. 163, p. 108105, 2022.

[18] W. Li et al., "Fault diagnosis of rotating machinery with a novel statistical feature extraction and evaluation method," *Mech. Syst. Signal Process.*, vol. 50, pp. 414–426, 2015.

[19] N. Espinoza-Sepulveda and J. K. Sinha, "Parameter optimisation in the vibration-based machine learning model for accurate and reliable faults diagnosis in rotating machines," *Machines*, vol. 8, no. 4, p. 66, 2020.

[20] N. Espinoza-Sepulveda and J. K. Sinha, "Robust vibration-based faults diagnosis machine learning model for rotating machines to enhance plant reliability," *Maint. Reliab. Cond. Monit.*, vol. 1, no. 1, pp. 2–9, 2021.

[21] K. M. Almutairi and J. K. Sinha, "Experimental vibration data in fault diagnosis: a machine learning approach to robust classification of rotor and bearing defects in rotating machines," *Machines*, vol. 11, no. 10, p. 943, 2023.

[22] K. Luwei, *Vibration-Based Fault Identification for Rotor and Ball Bearing in Rotating Machines*. Manchester, UK: University of Manchester, 2022.

[23] N. E. Huang, *Hilbert-Huang Transform and Its Applications*, Vol. 16. Hackensack, NJ: World Scientific, 2014.